Revision

26th August 2013

Polymers of Intrinsic Microporosity in Electrocatalysis: Novel Pore Rigidity Effects and Lamella Palladium Growth

Fengjie Xia [1,2], Mu Pan [1], Shichun Mu [1], Richard Malpass-Evans [3], Mariolino Carta [3], Neil B. McKeown [3], Gary A. Attard [3], Ashley Brew [3], David J. Morgan [3], and Frank Marken *[2]

[1] *State Key Laboratory of Advanced Technology for Materials Synthesis and Processing, Wuhan University of Technology, 430070, China*

[2] *Department of Chemistry, University of Bath, Claverton Down, Bath BA2 7AY, UK*

[3] *School of Chemistry, Cardiff University, Cardiff CF10 3AT, UK*

To be submitted to Electrochimica Acta

(Special Issue ISE Meeting 2013 Pretoria)

Proofs to F. Marken

Email F.Marken@bath.ac.uk

Abstract

Two polymers (i) the polymer of intrinsic microporosity (or PIM) ethanoanthracene TB-PIM (P1, PIM-EA-TB, MW 70 kDa, BET surface area 1027 m^2g^{-1}) and (ii) the structurally less rigid polymer based on dimethyldiphenylmethane units (P2, BDMPM-TB, MW 100 kDa, BET surface area 47 m^2g^{-1}) are compared to highlight the benefits of the newly emerging PIM membrane materials in electrocatalysis and nanostructure formation. Binding sites and binding ability/capacity in aqueous environments are compared in films deposited onto glassy carbon electrodes for (i) indigo carmine dianion immobilisation (weakly binding from water-ethanol) and (ii) $PdCl_4^{2-}$ immobilisation (strongly binding from acidic media). Nano-lamella growth for Pd metal during electro-reduction of $PdCl_4^{2-}$ is observed. Electrocatalytic oxidation of formic acid (at pH 6) is investigated for P1 and P2 as a function of film thickness. The more rigid high BET surface area PIM material P1 exhibits "open-pore" characteristics with much more promising electrocatalytic activity at Pd lamella within polymer pores.

Keywords: microporosity; nanostructure; fuel cell; formic acid; electrocatalysis.

1. Introduction

Polymers of intrinsic microporosity (PIMs) have emerged over the past decade [1,2] with potential applications in gas storage [3,4], in membrane separations [5,6,7], in heterogeneous catalysis [8], and as the active component for optical sensors [9]. The rigid and contorted polymer backbone of PIMs precludes efficient packing to generate novel properties due to permanent microporosity. To date, applications are all reliant on rapid molecular permeability, however, here we report the significance of intrinsic microporosity to facilitate rapid ion transport within electrochemical membranes, which may find application in a variety of devices including fuel cells [10].

Recently, the novel preparation of amine-containing PIMs based on a polymerisation reaction involving the formation of Tröger's base (TB) was reported [11]. Thus, 2,6(7)-diamino-9,10-dimethyl-ethanoanthracene was polymerised with dimethoxymethane in TFA to give PIM-EA-TB (P1, see Figure 1). Similarly, the commercially available monomer, bis(4-amino-3-methylphenyl)methane, reacts to give polymer BDMPM-TB (P2) with TB linking groups. Both polymers have similar chemical functionality (see Figure 1), are obtained with high molecular mass (M_w >70,000 g mol^{-1}), and are highly soluble in chloroform. However, only P1 demonstrates intrinsic microporosity with an apparent BET surface area of 1027 m^2 g^{-1} due to its highly rigid structure, as determined by nitrogen adsorption of powdered samples at 77 K. In contrast, P2 is non-porous (BET surface area = 47 m^2 g^{-1}) due to greater chain flexibility.

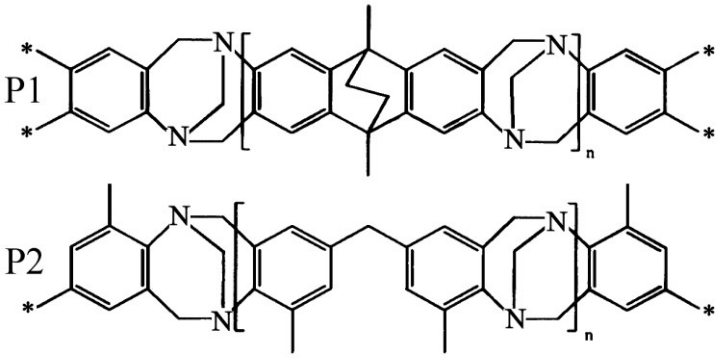

Figure 1. Scheme of molecular structures of P1 (PIM-EA-TB) and P2 (BDMPM-TB).

In this report these two polymers are compared when deposited as thin film on glassy carbon electrode surfaces. It is demonstrated that the design of polymer membranes with intrinsic microporosity has a considerable effect on the uptake and retention of redox active anions. Indigo carmine and $PdCl_4^{2-}$ are investigated. Nano-lamella-like growth of palladium metal within PIM pores is observed. The electrocatalytic activity of palladium metal within pores is contrasted. The rigid backbone of the PIM P1 is shown to provide active pores and good catalytic performance.

2. Experimental

2.1. Chemical Reagents

Polymers PIM-EA-TB (P1, M_W = 70 kDa, BET surface area = 1027 m^2 g^{-1}) and BDMPM-TB (P2, M_W = 100 kDa, BET surface area = 47 m^2 g^{-1}) were prepared from the trifluoroacetic acid (TFA) mediated reaction between dimethoxymethane and 2,6(7)-diamino-9,10-dimethyl-ethanoanthracene or bis(4-amino-3-methylphenyl)-

methane, respectively, as reported previously [11]. Formic acid, palladium dichloride, perchloric acid (70%), hydrochloric acid (30%), chloroform, ethanol, sodium hydroxide, and phosphoric acid (85 %) were obtained from Aldrich or Fisher Scientific and used without further purification. Solutions were prepared with filtered/deionised water of resistivity 18.2 MΩ cm from a Thermo Scientific water purification system (Barnstead Nanopure). Nitrogen was employed to de-aerate solutions prior to measurements.

2.2. Instrumentation

An Autolab potentiostat system (PGSTAT12, EcoChemie, The Netherlands) was employed with glassy carbon working electrode (3 mm diameter, BAS), a Pt wire counter electrode, and a KCl-saturated calomel reference (SCE, Radiometer, Copenhagen).

2.3. Procedures

The polymers P1 or P2 were completely dissolved into chloroform (1 mg in 1 mL solvent) by ultrasonication for 15 minutes. PIM films on glassy carbon electrodes were prepared by deposition of typically 5 μL solution and solvent evaporation. For indigo carmine experiments PIM or polymer coated electrodes were immersed into indigo carmine in phosphate buffer pH 2 (50 vol % ethanol) and then transferred to aqueous phosphate buffer for voltammetry. For $PdCl_4^{2-}$ experiments, PIM or polymer coated electrodes were immersed into 0.5 M HCl solution containing 0.05 M $PdCl_2$, rinsing with water, and transferring into a clean 0.1 M perchloric acid solution for Pd electro-deposition. The PIM containing Pd –coated glassy carbon electrode was then

transferred into 0.1 M formic acid in 0.1 M phosphate buffer solution pH 6 for measurements.

3. Results and Discussion

3.1. Effects of Intrinsic Microporosity I.: Indigo Carmine Uptake and Reactivity

In order to investigate the electrochemical properties of PIM versus non-porous polymer films, solutions in chloroform (1 mg in 1 mL) were deposited onto 3 mm diameter glassy carbon electrodes and evaporated to dryness to give polymer film deposits. Comparison of voltammetric responses for films of P1 and P2 materials alone suggest no intrinsic electrochemical responses (*vide infra*). However, the microporous films are able to incorporate redox active anions (to complement the intrinsic ammonium cation charge in the polymer backbone) such as indigo carmine. When PIM films are immersed into 1 mM indigo carmine in water, no significant uptake occurs (based on voltammetry). Similarly, a free-standing PIM film is not coloured under these conditions.

There are two methods of "opening pores" or "swelling" PIM materials for the more rapid exchange/uptake of anions such as indigo carmine: (i) addition of organic solvent such as ethanol or (ii) employing more acidic solution conditions. Both can be employed successfully for the immobilisation of indigo carmine. Figure 2A-C show how indigo carmine at pH 2 (in the presence of 50 vol% ethanol) can be used to colour a free-standing (ca. 60 μm thickness) P1 membrane.

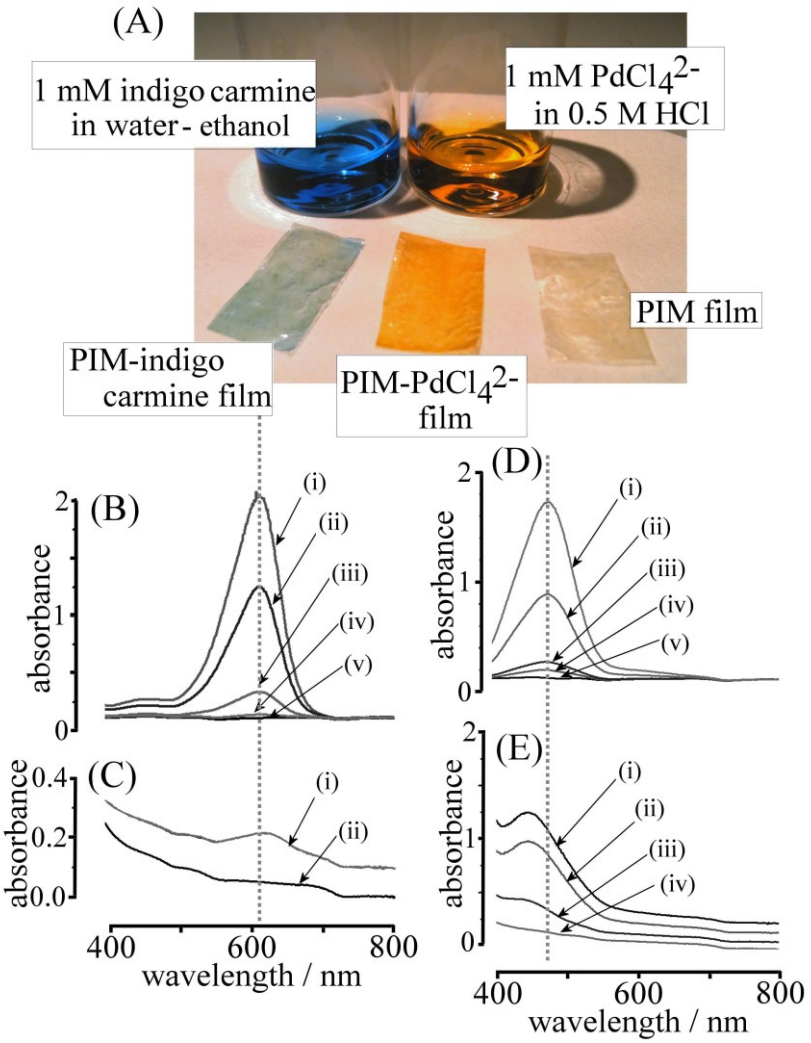

Figure 2. (A) Photograph of a blue solution of indigo carmine and a yellow solution of $PdCl_4^{2-}$ as well as P1 membranes before and after immobilisation of the redox active colorants. (B) UV/Vis spectra for (i) 100, (ii) 50, (iii) 10, (iv) 1, and (v) 0 μM indigo carmine in water-ethanol. (C) UV/Vis spectra for P1 film (ca. 60 μm) after immersion in (i) 10 and (ii) 0 mM indigo carmine in pH 2 buffer. (D) UV/Vis spectra for (i) 10, (ii) 5, (iii) 1, (iv) 0.5, and (v) 0 mM $PdCl_4^{2-}$ in 0.5 M HCl. (E) UV/Vis spectra for a P1 film (ca. 60 μm) after immersion in (i) 10, (ii) 5, (iii) 1, and (iv) 0 mM $PdCl_4^{2-}$ solution.

The extinction coefficient for indigo carmine monomer ε_{IC} = 20000 $M^{-1}cm^{-1}$ in solution [12] allows an estimate for the concentration of indigo carmine in the P1 membrane to be obtained (assuming a constant ε_{IC}). Based on data in Figure 2C the apparent concentration of indigo carmine in the P1 film is ca. 0.8 mM. This compares

to the apparent concentration of cationic binding sites estimated as 2.5 M (see structure in Figure 1; assuming a density of about 1 g cm^{-3}). Binding of indigo carmine under these conditions appears to be dominated by factors other than electrostatic or only a fraction of the Tröger base sites are protonated/accessible (*vide infra*).

The voltammogram in Figure 3Aiii shows the reduction and back-oxidation of indigo carmine in P1 immobilised by immersion into a 1 mM solution in 50-50 water-ethanol (see equation 1).

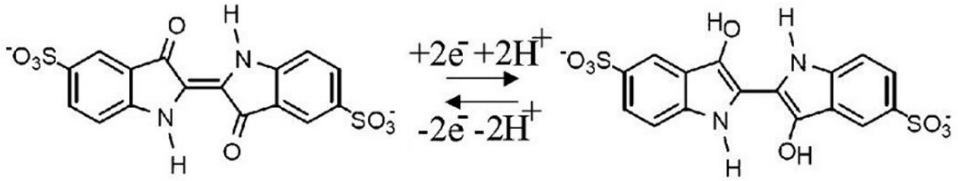

(1)

The reversible potential for the indigo carmine reduction is observed at E_{mid} = ½ ($E_{p,red}$ + $E_{p,ox}$) = -0.12 V vs. SCE (with ca. 60 mV peak-to-peak separation at 50 mVs^{-1}) which is shifted negative by about 55 mV with respect to the E_{mid} value for indigo carmine without PIM deposit (see dashed line). This negative shift is indicative of a stabilisation of indigo carmine with respect to leuco-indigo carmine (here leuco-indigo formation is likely to be associated with additional cation uptake into the PIM film).

Figure 3B shows the effect of changing the amount/thickness of the P1 film deposit. Only insignificant variation is observed indicative of a thin active region of P1 film close to the electrode surface. This is confirmed in the scan rate dependence of peak

currents for the voltammetric responses (see Figure 3C), which is consistent with a square root dependence and therefore semi-infinite charge diffusion within a thin layer in the polymer film (not shown).

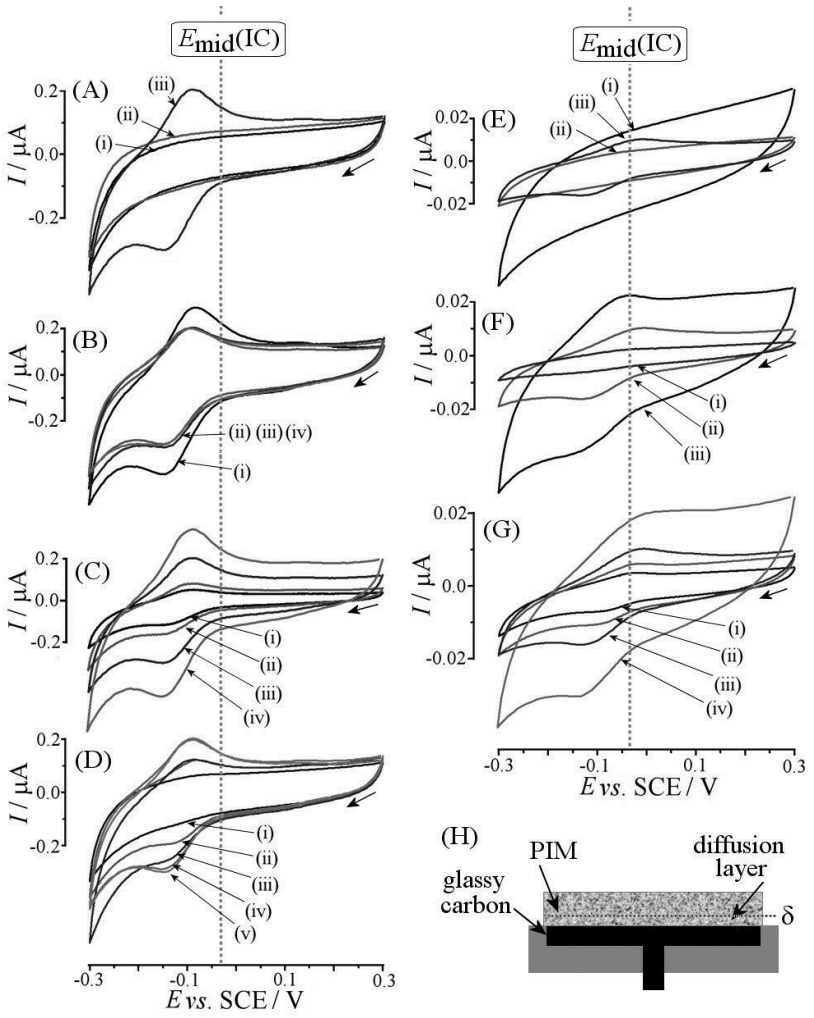

Figure 3. (A) Cyclic voltammograms (3 mm diameter glassy carbon with 5 µg P1 deposit, scan rate 50 mV s^{-1}) immersed in 0.1 M PBS pH 2 for (i) no treatment, (ii) one minute immersion into 10 mM indigo carmine in water, and (iii) 5 minutes immersion into 10 mM indigo carmine in 50-50 water-ethanol. (B) Conditions as in Aiii, but for (i) 2, (ii) 5, (iii) 10, and (iv) 15 µg P1. (C) Conditions as in Aiii, but scan rate (i) 10, (ii) 20, (iii) 50, and (iv) 100 mVs^{-1}. (D) Conditions as in Aiii, but 5 minute immersion into 50-50 water-ethanol with (i) 0.05, (ii) 0.1, (iii) 1, (iv) 5, and (v) 10 mM indigo carmine. (E) Cyclic voltammograms (3 mm diameter glassy carbon with 5 µg P2 deposit, scan rate 50 mV s^{-1}) immersed in 0.1 M PBS pH 2 for (i) no treatment, (ii) 5 minute immersion into 10 mM indigo carmine in water, and (iii) 5 minute immersion into 10 mM indigo carmine in 50-50 water-ethanol. (F) Conditions as in Eiii, but for (i) 10, (ii) 5, and (iii) 2 µg P2. (G) Conditions as in Eiii, but scan rate (i) 10, (ii) 20, (iii) 50, and (iv) 100 mVs^{-1}. Dashed lines indicate the midpoint potential E_{mid}(IC) for indigo carmine in the absence of PIM. (H) Schematic depiction of the modified electrode with internal diffusion layer δ.

The effect of the indigo carmine concentration on the immobilisation process are shown in Figure 3D. A concentration effect on the indigo carmine uptake is observed consistent with a Langmuirian binding constant estimated as $K_{IC} = 10^4$ $mol^{-1}dm^3$ (for water-ethanol 50-50, assuming that the indigo carmine concentration at the point of half-filled sites can be inverted to give an estimate for K_{IC}).

The same range of experiments was performed with the P2 polymer with substantially lower BET surface area and a dramatic difference is immediately apparent. Data in Figure 3E shows that P2 is actually changing the double layer capacitance presumably by more effectively blocking the electrode surface (less open porosity). The indigo carmine redox process is observed again when immobilised from 50-50 water-ethanol, but the charge under the reduction peak is much lower (here ca. 0.02 μC for P2 compared to 0.4 μC for P1). The ratio of peak charge for P2 to P1 is not dissimilar to the ratio of BET surface area and likely to be linked to the structural access to the interior of the polymer.

The midpoint potential for the reduction of indigo carmine in the P2 polymer deposit is shifted negative by ca. 25 mV, which may indicate stronger binding of indigo carmine relative to leuco-indigo carmine or also be linked to a local change in pH within pores during redox cycling. In all cases the electrochemical process occurs within a thin charge diffusion zone δ as shown in Figure 3H.

3.2. Effects of Intrinsic Microporosity II.: $PdCl_4^{2-}$ Uptake and Reactivity

In order to explore a wider range of micro-pore effects in P1 and P2, the uptake and reduction of $PdCl_4^{2-}$ are investigated next. Absorption of $PdCl_4^{2-}$ from aqueous hydrochloric acid is facile and does not require the addition of ethanol. The interaction of $PdCl_4^{2-}$ with organic ammonium cations has been reported to occur mainly via hydrogen bonds [13]. The photograph in Figure 2A shows the strong coloration of a free-standing P1 membrane after immersion into $PdCl_4^{2-}$ solution in hydrochloric acid. From UV/Vis spectra (see Figure 2D and E) it can be seen that a similar peak in the absorbance is observed, which (for $\varepsilon_{Pd(II)}$ = 160 $M^{-1}cm^{-1}$) allows the apparent concentration for $PdCl_4^{2-}$ in P1 to be estimated as ca 0.8 M. Given that there are two negative charges on each $PdCl_4^{2-}$ and that geometric constraints will limit the total number of ammonium binding sites within P1, this value is consistent with a complete saturation of the electrostatic binding sites (estimated as 2.5 M). $PdCl_4^{2-}$ is bound very effectively. Similar experiments with P2 suggest much weaker coloration consistent with a much lower number of active binding sites (therefore substantially less porosity).

Figure 4A shows typical cyclic voltammograms (5^{th} cycle) for a bare glassy carbon (i) and for a P1 modified glassy carbon after immersion into $PdCl_4^{2-}$. Binding of Pd(II) into the porous P1 material leads to the formation of Pd metal deposits at the glassy carbon electrode – PIM interface within the P1 film.

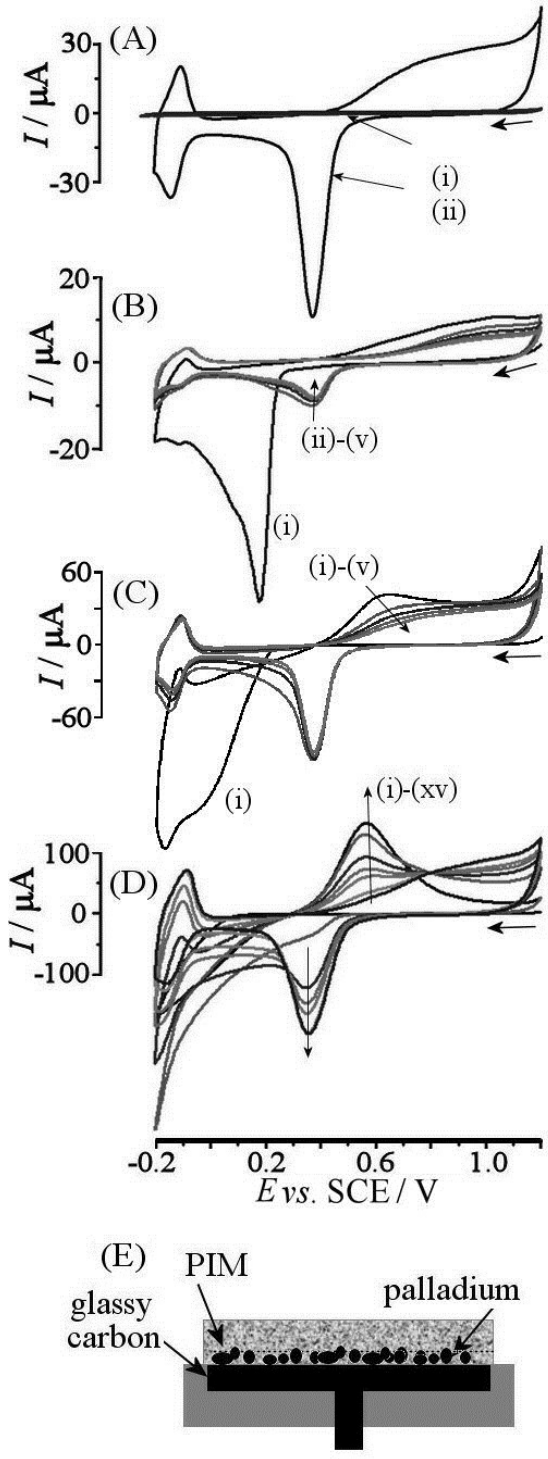

Figure 4. (A) Cyclic voltammograms (5th cycle, scan rate 50 mVs^{-1}) in 0.1 M $HClO_4$ for (i) a bare electrode after immersion into 25 mM $PdCl_4^{2-}$ / 0.1 M HCl, and (ii) a 5 μg P1 modified electrode after immersion into 25 mM $PdCl_4^{2-}$ / 0.1 M HCl. (B) Multi-cycle experiment (5 cycles) for a 5 μg P1 deposit after immersion into 0.5 mM $PdCl_4^{2-}$ / 0.1 M HCl. (C) Multi-cycle experiment (5 cycles) for a 5 μg P1 deposit after immersion into 25 mM $PdCl_4^{2-}$ / 0.1 M HCl. (D) Multi-cycle experiment (15 cycles) for a 10 μg P1 deposit after immersion into 25 mM $PdCl_4^{2-}$ / 0.1 M HCl. (E) Schematic drawing of the Pd deposit forming at the electrode – PIM interface.

The amount of P1 deposited onto the glassy carbon electrode surface affects the shape of the developing Pd surface response. In the first potential cycle reduction is observed (see Figure 4Bi for 0.5 mM $PdCl_4^{2-}$ and Figure 4Ci for 25 mM $PdCl_4^{2-}$) which is then followed by formation of two stable voltammetric responses. At E_{mid} = -0.12 V vs. SCE the hydrogen adsorption signal (approximately 0.6 V negative of the onset of the oxide region) is observed characteristic for palladium surfaces [14]. At ca. 0.5 V vs. SCE the oxidation/reduction of the palladium surface is observed. Thicker deposits of P1 appear to lead to much higher surface area palladium deposits (see Figure 4D). The process is likely to be confined in a film or islands at the polymer – electrode interface (see Figure 4E).

In Figure 5 data for films of P1 and P2 are compared. The cyclic voltammetry response for the Pd deposit formed in aqueous 0.1 M $HClO_4$ is affected by the amount of PIM or polymer material at the electrode surface. Figure 5A and 5C show data for P1 and P2, respectively, and the linear increase in both cases suggests that Pd(II) from the film is converted Pd metal with increasing surface area as the amount of PIM is increased. The charge under the reduction peak at 0.38 V vs. SCE is used to compare Pd surface area and the peak charge for P1 appears to be an order of magnitude higher consistent with the higher BET surface area (adsorption capacity) of the polymer.

The investigation of the effect of the $PdCl_4^{2-}$ concentration on the absorption process is shown in Figure 5E. At concentrations of ca. 10 mM for P1 and 30 mM for P2 a plateau is reached and the PIM or polymer appears saturated with $PdCl_4^{2-}$. Apparent

Langmuirian binding constants for P1 and P2 can be estimated as ca. $K_{Pd(II)}$ = 1000 $mol^{-1}dm^3$ and 100 $mol^{-1}dm^3$, respectively. These are lower compared that that for indigo carmine (*vide supra*) probably reflecting the more acidic 0.5 M HCl environment during binding and the more hydrophilic nature of the guest.

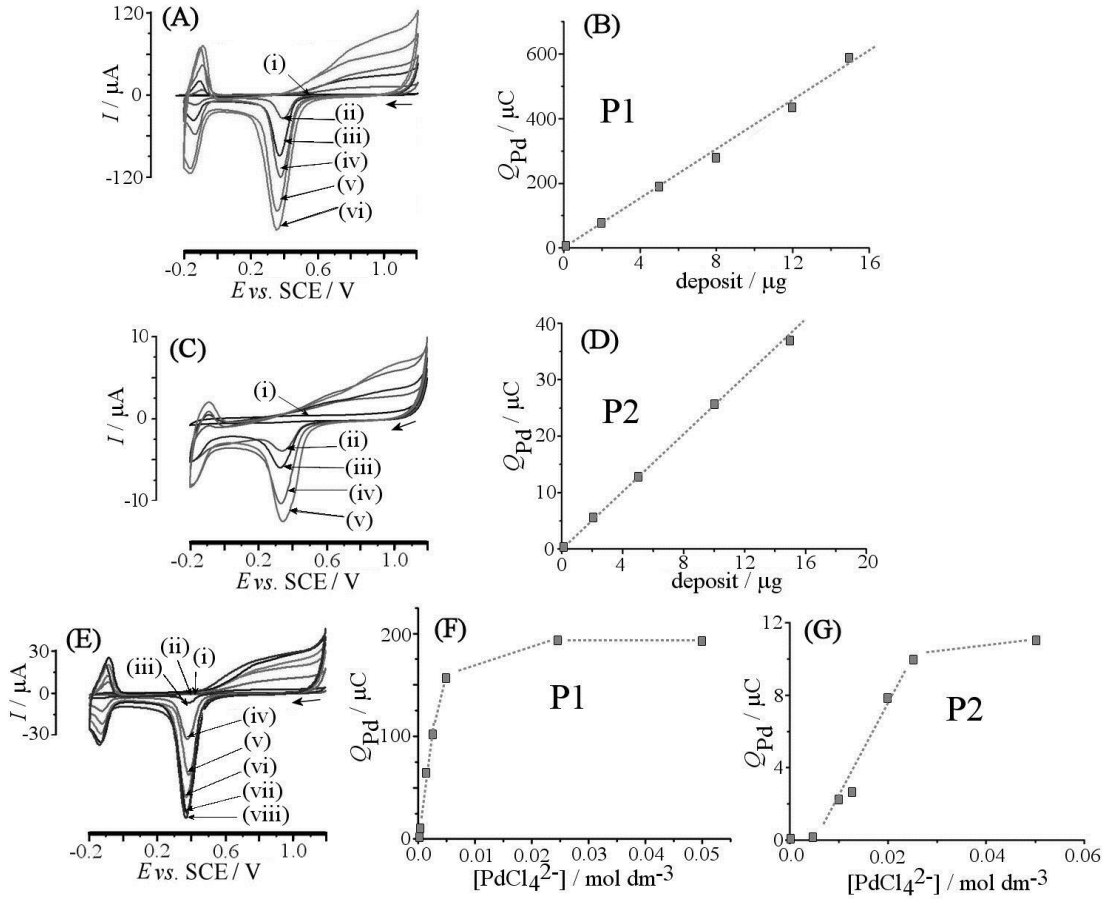

Figure 5. (A) Cyclic voltammograms (5th cycle, scan rate 50 mVs^{-1}, in 0.1 M $HClO_4$) for P1 on glassy carbon for (i) 0, (ii) 2, (iii) 5, (iv) 8, (v) 12, and (vi) 15 µg films after absorption of $PdCl_4^{2-}$. (B) Plot of the charge under the reduction peak at 0.38 V vs. SCE versus amount of P1 deposit. (C) Cyclic voltammograms (5th cycle, scan rate 50 mVs^{-1}, in 0.1 M $HClO_4$) for P2 on glassy carbon for (i) 0, (ii) 2, (iii) 5, (iv) 10, and (v) 15 µg films after absorption of $PdCl_4^{2-}$. (D) Plot of the charge under the reduction peak at 0.38 V vs. SCE versus amount of P2 deposit. (E) Cyclic voltammograms (5th cycle, scan rate 50 mVs^{-1}, in 0.1 M $HClO_4$) for P1 on glassy carbon for 5 µg films after absorption of (i) 0, (ii) 0.1, (iii) 0.5, (iv) 1.5, (v) 2.5, (vi) 5, (vii) 25, and (viii) 50 mM $PdCl_4^{2-}$. (F) Plot of the charge under the reduction peak at 0.38 V vs. SCE versus $PdCl_4^{2-}$ concentration for P1. (G) As before but for P2.

The increase in the palladium surface area in particular for higher levels of deposit of P1 appear promising in view of improved catalytic properties. Additional experiments were performed with P1 films saturated with $PdCl_4^{2-}$, then reduced to Pd, and then saturated with $PdCl_4^{2-}$ again, and so on. Perhaps surprisingly, this did not lead to further increases in Pd surface area (as judged by the area under the peak at 0.4 V vs. SCE, see Figure 5A).

Next, the direct deposition of Pd into 5 μg P1 from a solution of 1 mM $PdCl_4^{2-}$ in 0.1 M HCl was attempted. The resulting Pd metal deposit shows voltammetric features in 0.1 M $HClO_4$ similar to the Pd deposits in Figure 5A. Figure 6A shows that an increase in the Pd surface area with deposition time occurs. The comparison of the voltammetric responses with that in Figure 4Aii suggests that this continuing deposition is not very effective in providing a higher surface area Pd deposit and this can be rationalised when studying the electron optic images in Figure 6B-D. Nano-lamella palladium can be seen densely packed within the polymer matrix with a thickness of less than 50 nm per lamella. The reason for the lamella growth is likely to be connected to the binding of the ammonium functional groups in the polymer to the growing Pd surface in a way that leads to restricted 2D sheet growth (e.g. for polymer "Cumberland-coils"; see structure in Figure 1). The dense packing of the lamella is likely to create active palladium surface only on the outside of grains. In the continuing deposition (Figure 6) only little extra surface area is created (see drawing in Figure 6E). However, under conditions in Figure 5A new grains or islands of lamella may form in the initial stages thereby rapidly adding to the active surface area.

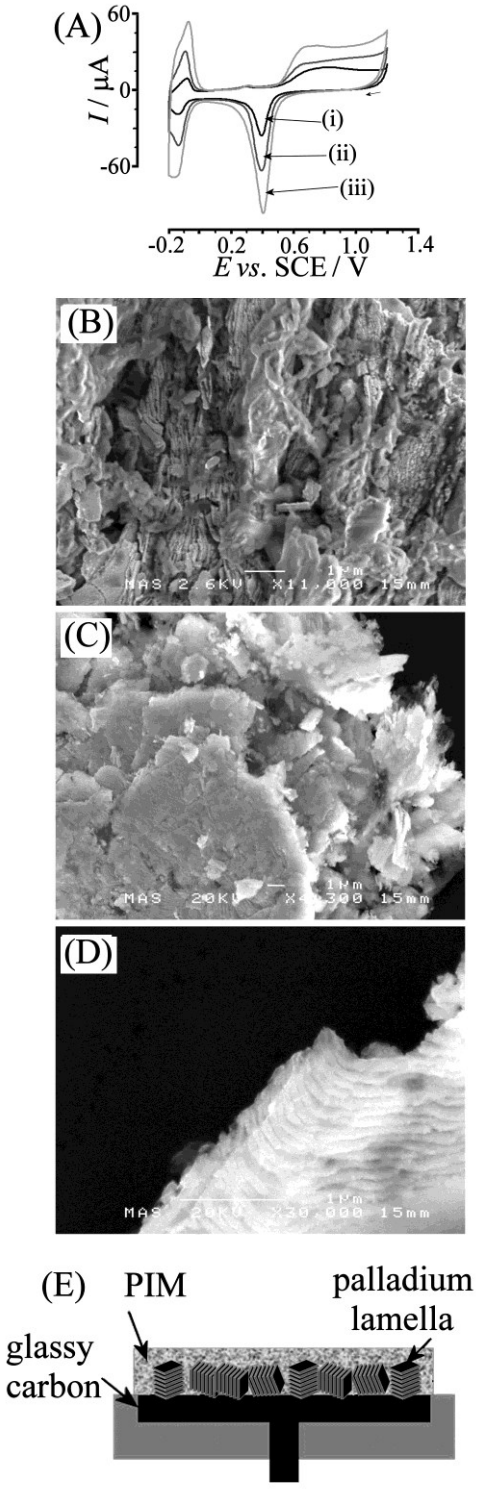

Figure 6. (A) Cyclic voltammograms (scan rate 50 mVs^{-1}) for a 5 μg P1 deposit immersed in 0.1 M $HClO_4$ after continuous electro-deposition of Pd from 1 mM $PdCl_4^{2-}$ in 0.1 M HCl at 0.0 V vs. SCE for (i) 150, (ii) 500, and (iii) 1200 s. (B,C,D) FE-SEM images for the 1200 s deposit. B shows a top view and C,D show film fragments scraped off the original film electrode. (E) Schematic drawing of the lamella formation in films or islands at the electrode surface.

From the PIM-absorbed $PdCl_4^{2-}$ interesting palladium nano-metal deposits with lamella morphology can be formed within pores and therefore the catalytic activity could be affected by the PIM matrix. In the next section the Pd-catalytic oxidation of formic acid is investigated in order to explore PIM polymer pore effects.

3.3. Effects of Intrinsic Microporosity III: Formic Acid Oxidation Electrocatalysis

The oxidation of formic acid at Pd catalysts is important in the development of formic acid fuel cells [15]. We have recently shown [16] that this process is improved when going to less acidic media such as aqueous buffer at pH 6 and that gaseous CO_2 may play a major role in slowing down the rate of this process. Here the reactivity of formic acid in pores of P1 filled with Pd is investigated.

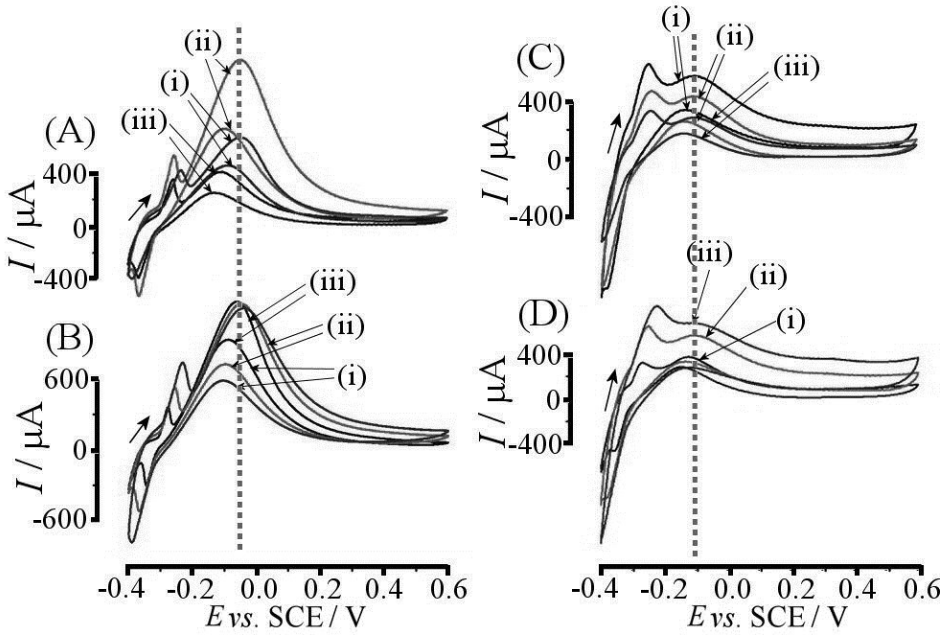

Figure 7. (A) Cyclic voltammograms (scan rate 50 mVs^{-1}) for (i) 2, (ii) 5, (iii) 10 μg P1 with Pd formed in 0.1 M formic acid / 0.1 M PBS pH 6. (B) As above, for 5 mg P1 but scan rate (i) 20, (ii) 50, and (iii) 100 mVs^{-1}. (C) As in A for P2. (D) As in B but for 2 μg P2. Dashed line indicates formic acid oxidation signal.

Figure 7A shows data for the oxidation of formic acid when (i) 2, (ii) 5, and (iii) 10 μg P1 is deposited, saturated with $PdCl_4^{2-}$, cycled to form the Pd catalyst, and immersed into 0.1 M formic acid at pH 6. The formic acid oxidation peak occurs during forward and backward scan at ca. -0.05 V vs. SCE for P1 which is consistent with the catalytic oxidation to carbon dioxide (see equation 2 [16]).

$$Pd + HCOOH \rightarrow Pd + CO_2 + 2\,H^+ + 2\,e^- \qquad (2)$$

Initially, an increase in the oxidation peak response is seen when going to 5 μg P1 deposit. Then however, further increase in the amount of P1 decreases the oxidation peak. Although the active Pd surface is expected to increase (see Figure 5A) the additional polymer membrane is slowing down access for reagents and removal of products. When inspecting the scan rate dependence for this process (see Figure 7B) it can be seen that the surface redox responses for hydrogen on Pd centered at -0.3 V vs. SCE increase proportional to scan rate (as expected for surface confined processes) whereas the formic acid oxidation peak remains close to constant (consistent with a process limited by a preceding chemical step or membrane transport).

Similar experiments were conducted with polymer P2 (see Figure 7C and D) and an entirely different type of behaviour was observed. The increase in the amount of P2 deposit decreases the catalytic peak and although the surface confined peaks centered at -0.3 V vs. SCE are increased compared to those for P1 (see Figure 7A) the catalytic response is substantially smaller. This can be explained with the absence of effective pores in the P2 film blocking the catalytic process.

Overall, a dramatic difference in reactivity is observed when comparing the rigid high BET area P1 material with the more flexible low BET P2. Catalytic processes within the P1 pores are possible when the film thickness is limited. In future pore-electrocatalysis could be a very interesting alternative to "open" nanoparticle catalysis due to the potential to control reactions (selectivity, chirality) and to stablilise the catalyst (e.g. avoiding migration and Ostwald ripening by polymer containment [17,18]).

4. Conclusions

It has been demonstrated that polymers of intrinsic microporosity (PIMs) provide a new and very interesting component for electrochemical systems. The rigid pores provide accessible nano-pores for reagent and ion diffusion and the characteristics are very different when compared to traditional less rigid polymer systems. The P1 materials (PIM-EA-TB) has ammonium cations embedded in the rigid structure and thereby becomes permselective to anions such as $PdCl_4^{2-}$. PIMs will open up a range of new opportunities for the selective transport of reagents and improved stability in nano-catalyst systems, they provide a new generation of nano-templates for example for lamella-like growth, and they have potential to revolutionise the design of other types of electrochemical interfaces.

Acknowledgements

This work was supported by CSC (China Scholarship Council, File No. 2010695033).

References

[1] P. M. Budd, B. S. Ghanem, S. Makhseed, N. B. McKeown, K. J. Msayib, C. E. Tattershall, Chem. Commun. (2004) 230.

[2] N. B. McKeown, P. M. Budd, Macromolecules 43 (2010) 5163.

[3] N. B. McKeown, P. M. Budd, Macromolecules 43 (2010) 5163.

[4] N. B. McKeown, B. Gahnem, K. J. Msayib, P. M. Budd, C. E. Tattershall, K. Mahmood, S. Tan, D. Book, H. W. Langmi, A. Walton, Angew. Chem. Int. Ed. 45 (2006) 1804.

[5] S.V. Adymkanov, Y.P. Yampol'skii, A.M. Polyakov, P.M. Budd, K.J. Reynolds, N.B. McKeown, K.J. Msayib, Polymer Sci. 50 (2008) 444.

[6] P. M. Budd, N. B. McKeown, B. S. Ghanem, K. J. Msayib, D. Fritsch, L. Starannikova, N. Belov, O. Sanfirova, Y. P. Yampol'skii, V. Shantarovich, J. Membr. Sci. 325 (2008) 851.

[7] C. G. Bezzu, M. Carta, A. Tonkins, J.C. Jansen, P. Bernardo, F. Bazzarelli, N. B. McKeown, Adv. Mater. 24 (2012) 5930.

[8] H.J. Mackintosh, P.M. Budd, N.B. McKeown, J. Mater. Chem. 18 (2008) 573.

[9] Y. Wang, N.B. McKeown, K.J. Msayib, G.A. Turnbull, I.D.W. Samuel, Sensors 11 (2011) 2478.

[10] D.J.L. Brett, A.R. Kucernak, P. Aguiar, S.C. Atkins, N.P. Brandon, R. Clague, L.F. Cohen, G. Hinds, C. Kalyvas, G.J. Offer, B. Ladewig, R. Maher, A. Marquis, P. Shearing, N. Vasileiadis, V. Vesovic, ChemPhysChem 11 (2010) 2714.

[11] M. Carta, R. Malpass-Evans, M. Croad, Y. Rogan, J. C. Jansen, P. Bernardo, F. Bazzarelli, N. B. McKeown, Science 339 (2013) 303.

[12] B. Shen, M. Olbrichstock, J. Posdorfer, R.N. Schindler, Zeitsch. Phys. Chem.-Inter. J. Res. Phys. Chem. Chem. Phys. 173 (1991) 251.

[13] A. Bencini, A. Bianchi, P. Dapporto, E. Garciaespana, M. Micheloni, P. Paoletti, P. Paoli, Chem. Commun. (1990) 753.

[14] M. Hara, U. Linke, Th. Wandlowski, Electrochim. Acta 52 (2007) 5733.

[15] N.V. Rees, R.G. Compton, J. Solid State Electrochem. 15 (2011) 2095.

[16] N.C. Cheng, R.A. Webster, M. Pan, S.C. Mu, L. Rassaei, S.C. Tsang, F. Marken, Electrochim. Acta 55 (2010) 6601.

[17] H.L. Xin, J.A. Mundy, Z.Y. Liu, R. Cabezas, R. Hovden, L.F. Kourkoutis, J.L. Zhang, N.P. Subramanian, R. Makharia, F.T. Wagner, D.A. Muller, Nano Lett. 12 (2012) 490.

[18] F.J. Xia, M. Pan, S.C. Mu, M.D. Jones, G. Kociok-Köhn, S.C. Tsang, F. Marken, Electrochim. Acta (2013) doi.org/10.1016/j.electacta.2013.01.014.